INDIAN OCEAN REVIEW OF SCIENCE AND TECHNOLOGY
ISSN: 2312-1874, Article 3-2013

Optoelectronics and vibrational properties of carbidopa from quantum chemistry computations

N. F. Frazão[1], E. L. Albuquerque[1]*, U. L. Fulco[1], P. W. Mauriz[2], D. L. Azevedo[3]

Abstract
DOPA Decarboxylase (DDC) is an enzyme responsible for the synthesis of the neurotransmitter dopamine, which is performed metabolizing levodopa by decarboxylation reaction. It has being active in several clinic disorders, including Parkinson's disease. Carbidopa (CDOPA) is a peripheral inhibitor of DDC that is ingested together with the levodopa, being the antiparkinsonian drug most used nowadays. Aiming to give a quantum chemistry theoretical description of the carbidopa molecule, we present here its geometrical, optoelectronic, and vibrational spectroscopic results. Annealing calculations were employed to explore the space of the molecular geometry of carbidopa, in order to obtain its most stable conformations of smaller energies by using density functional theory (DFT) with the LDA/PWC, GGA/PBE, and GGA/BLYP functionals. The carbidopa's structural data (bond length, bend, and torsion angle), charge population analysis (absorption spectra), and molecular orbital study (HOMO, LUMO, PDOS, and DOS) are then obtained considering one of its smallest conformation energy. Furthermore, a detailed interpretation of the carbidopa harmonic vibrational frequencies are here also presented, through the analysis of its infrared (IR) and Raman scattering spectroscopy.

Keywords
Peripheral inhibitor — Biological application — Density Functional Theory — Infrared — Raman

[1] *Departamento de Biofísica e Farmacologia, Universidade Federal do Rio Grande do Norte, 59072-970 Natal-RN, Brazil*
[2] *Departamento de Física, Instituto Federal de Educação, Ciência e Tecnologia do Maranhão, 65030-005 São Luís-MA, Brazil*
[3] *Departamento de Física, Centro de Ciências Exatas e Tecnologia, Universidade Federal do Maranhão, 65085-580 São Luís-MA, Brazil*
***Corresponding author**: eudenilson@gmail.com

Contents

1. Introduction

Parkinson's disease (PD) is a progressive, neurodegenerative disorder of the extrapyramidal nervous system characterized by the loss of nigrostriatal dopaminergic neurons (dopamine), which affects the mobility and control of the skeletal muscular system [Lloyd *et al*, 1970] and [Fahn *et al*, 1971]. This condition causes tremor, muscle stiffness or rigidity, slowness of movement (bradykinesia) and loss balance.

Although extremely necessary, unfortunately the dopamine cannot be ingested directly by the patients, because their blood-brain barrier (BBB) do not allow its cross transport into the brain. One effective way to overcome this problem is to consider alternatively the administration of the oral dopamine precursor levodopa, which is capable of BBB crossing and is converted into dopamine by the enzyme DOPA decarboxylase, mainly to patients at the initial stages of the disease.

Notwithstanding, levodopa is usually administered combined with carbidopa, chemically known as (2S)-3-(3,4-dihydroxyphenyl)-2-hydrazinyl-2-methylpropanoic acid, whose chemical formula is $C_{10}H_{16}N_2O_5$ [Calne, 1993]. Carbidopa prevent the breakdown of levodopa in the bloodstream, and also delays the conversion of levodopa into dopamine until it reaches the brain, reducing adverse side effects [Gilbert *et al*, 2000]. Furthermore, it can decrease peripheral aromatic L-amino acid decarboxylase (AADC) before it cross the BBB, metabolized by an enzymatic reaction of levodopa, resulting in a greater amount of levodopa dose to be transported to the brain, with the scope to compensate the deficiency of dopamine. It improves also the transport of levodopa across the BBB, reducing fluctuations in plasma and brain levels of levodopa, and avoiding the exposure of the brain dopamine receptors to alternating low and high concentration of dopamine [Mazloum-Ardakani *et al*, 2011], [Olanow *et al*, 2001] and [Nascimento *et al*, 2008].

In previous work we studied the development of carrier systems to increase the rate of LDOPA crossing the BBB, to achieve stable therapeutic plasma levels and minimize side

effects, has been a challenge. Innovative nanosystems for delivering LDOPA are being tested for improved Parkinson's disease therapy. In particular, buckminsterfullerene C_{60} is promising, due to its ability to penetrate through the skin and the gastrointestinal tract, as well as its biomedical applications to enhance drug delivery. Aiming to give theoretical support to attempts in developing levodopa preparations for transdermal and oral administration that may provide more continuous dopamine stimulation and fewer side effects, we present a computational study of levodopa adsorption on C60 fullerene in the 2-8 pH range (for a quantum mechanical description of levodopa adsorbed in a C_{60} fullerene see Ref. [Frazao *et al*, 2012]).

The central aim of the present work can be divided into two parts:

(1) To provide detailed and accurate informations of the isolated carbidopa molecule.

(2) To use the results of the item 1 as a prerequisite to the development of future works related to the mechanisms of adsorption and drug delivery used in the PD therapy.

To achieve the first part of our goal, in the present work a detailed study of the conformational, structural, optoelectronic and vibrational spectroscopic properties was conducted through a description of quantum chemistry. It is important to emphasize that in the present study we are using the same methodology employed in our previous work [Frazao *et al*, 2012]. Another strong motivation for understanding the physical properties listed in item 1, is its importance in the PD therapy, since the carbidopa occupies a prominent place in current treatment protocols of this neurodegenerative disease. Our research group aims to develop efforts to prepare the complex CDOPA@C60 and to probe the vibrational signatures of the adsorption, this is in according to the second part of our goal described in item 2.

2. Methods

Boltzmann jump search method is used to find the conformers of smaller energy. The method is based on the Metropolis algorithm to explore conformational space for energy minima. Random perturbation is performed in torsional space while quenching is performed in Cartesian space [Kirkpatrick *et al*, 1983] and [Stefan, 2004]. The possible conformers with smaller minima energies are shown in Fig. 1. The Universal Force Field (UFF) [Rappe *et al*, 1992], [Casewit *et al*, 1992], [Casewit *et al*, 1992], and [Rappe *et al*, 1993] was selected to perform about one hundred of perturbation per jump for each initial geometry. We have adopted the temperature of 500 K to each jump; after that, the smallest energy configuration was optimized classically.

To perform the quantum optimization together with the optical and electronic calculations of the carbidopa, we have used the DMol^3 code [Delley, 1990] and [Delley, 2000] within the density functional theory (DFT) formalism [Hohenberg *et al*, 1964] and [Kohn *et al*, 1965] considering the local density approximation (LDA) [Kohn *et al*, 1965], [Jones *et al*, 1989], [Gritsenko *et al*, 1997] and the generalized gradient approximation (GGA) [Dal Corso *et al*, 1996], and [Fuchs *et al*, 1998] as the functionals of exchange-correlation. The LDA functional was used in its standard parametrization, as proposed by Perdew and Wang (PWC functional) [Perdew *et al*, 1992], while the GGA functional [Perdew *et al*, 1986] was considered in two parametrization, being one the Perdew-Burke-Ernzerhof (PBE functional) method [Perdew *et al*, 1996], while the other as proposed by Becke (BLYP functional) [Becke *et al*, 1988]. We do not adopted any pseudopotential calculation to replace the core electrons in each atomic species: all electrons were included in the calculation. Double numerical plus polarization basis set (DNP) was adopted to expand the Kohn-Sham electronic eigenstates with an orbital cutoff radius of 3.5 Å.

The optimized structural parameters were used in the vibrational frequency calculations to characterize all stationary points as minima. We have utilized the gradient corrected DFT [Hohenberg *et al*, 1964] with the three-parameter hybrid functional (B3LYP, which mixes Hartree-Fock and DFT exchange energy terms) [Becke, 1993] for the exchange part, and the Lee-Yang-Parr (LYP) correlation function [Lee *et al*, 1988], looking for the vibrational frequencies of the optimized structures. Vibrational frequencies have been calculated at B3LYP/6-311G(d,p) basis set to expand the electronic states [Fast *et al*, 1999], enabling us to make the detailed IR and Raman assignments spectra of the carbidopa molecule. All DFT calculations are obtained by performing a geometrical optimization using the GAUSSIAN 09 code [Frisch *et al*, 2009] without any constraint on the geometry, whose convergence were: maximum force smaller than 7.7×10^{-4} eV/Å; self-consistent field energy variation smaller than 2.7×10^{-5} Å; and maximum atomic displacement smaller than 3.2×10^{-5} Å.

In systems with strong charge-transfer effects, contributions from electron density derivatives in the exchange-correlation functional improve the accuracy of the results [Santos *et al*, 2008], which is not the case of the one investigated here. Pure DFT methods are unable to provide a good description of systems where noncovalent bonding, such as van der Waals forces, are involved [Zhao *et al*, 2005], [Wijst van der *et al*, 2006], [Cooper *et al*, 2008], and [Silvestrelli, 2009]. Besides, hydrogen bonds are not well characterized by the LDA approximation. Nevertheless, some reports using DFT calculations to investigate layered crystals such as graphite, anhydrous DNA bases and guanine hydrated crystals show that the local density approximation (LDA) is adequate to obtain intermolecular distances [Ortmann *et al*, 2008], [Maia *et al*, 2011], [Ortmann *et al*, 2005], and [Ortmann *et al*, 2006]. Kee *et al.* [Kee *et al*, 2009], studying aromatic interactions in the binding of ligands in the active site of an enzyme, showed that the LDA functional agrees well with the more sophisticated MP2 method in comparison with generalized-gradient

approximation (GGA) and hybrid functionals (B3LYP).

The optical properties are analyzed through their optical absorption spectra. They were investigated by DFT calculations with LDA/PWC, GGA/PBE, and GGA/BLYP functionals, as implemented in the DMol^3 program. We used only the 25 lowest singlet states to calculate the optical properties. Knowing that the carbidopa molecule has closed-shell and is a non-periodic system, the calculations were performed using the RPA (Random Phase Approximation) method, neglecting the exchange-correlation response, but considering the electrostatic response. Gaussian integration was the broadening method used to calculate the optical spectrum with a value of 5.0 nm to the smearing width.

3. Results and Discussion

3.1 Geometry Optimization

The molecular conformers of carbidopa, that were obtained from Boltzmann jump search method of calculation, are shown in Fig. 1. The carbidopa molecule contains three radicals connected to the benzene ring, being one $C_4O_2N_2H_9$ and the others OH hydroxyl group [George *et al*, 1990]. The first radical is composed by four important groups, the so-called primary amine, secondary amine, carboxyl, and methyl. There are nine possible conformers of smaller energy for the carbidopa molecule.

The carbidopa in Fig. 1(a) is the conformer with the smallest energy ($E = -793.66117$ Ha), followed by the conformers in Fig. 1(b) to (i), with energies in the range $E = -793.65908$ Ha to $E = -793.64152$ Ha. These energies were obtained by geometry optimized carried out on the DMol^3 using DFT theory.

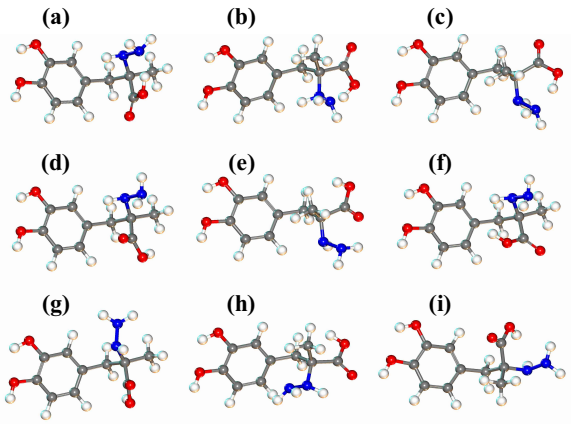

Figure 1. The carbidopa molecule conformations of smallest energy, where (a) $E = -793.66117$ Ha, (b) $E = -793.65908$ Ha, (c) $E = -793.65462$ Ha, (d) $E = -793.64962$ Ha, (e) $E = -793.64856$ Ha, (f) $E = -793.64820$ Ha, (g) $E = -793.64404$ Ha, (h) $E = -793.64237$ Ha, and (i) $E = -793.64152$ Ha.

The geometry with the smallest energy, obtained after the quantum calculation, is the most appropriated conformer chosen to represent the carbidopa from now on. The labels adopted to identify each atom of the carbidopa optimized geometry are showed in Fig. 2(a), and are quite important to analyze their structural measures. The $NHNH_2$ and COOH groups are positively and negatively charged, respectively. Fig. 2(b) shows the projection of the calculated electron density of carbidopa onto an electrostatic potential surface. From there, one can see that the most negatively charged atoms are the one labeled as O1 and O2, followed by O3 and O4. The most positively charged atoms are the Nitrogen N5 and N6, as well as the H17, H18, H19, H20, H2, and H22 hydrogen atoms; the ring and remaining carbon atoms are slightly positively charged.

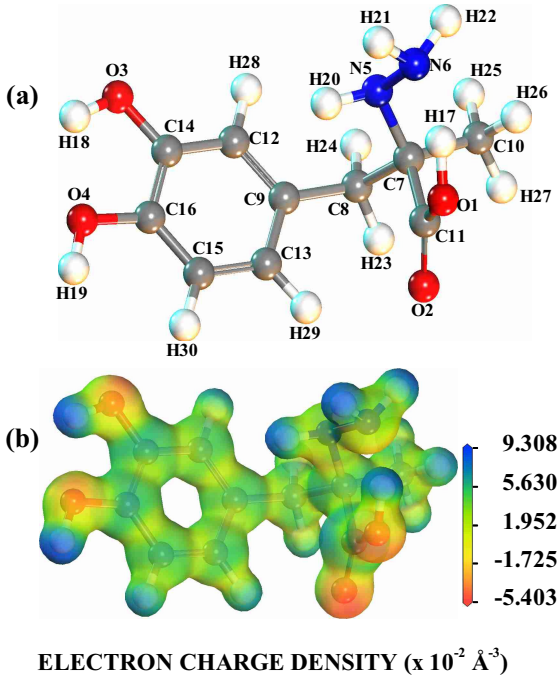

Figure 2. The carbidopa molecule of smallest energy. (a) Its most stable converged structure; (b) the electron density of its most stable converged structure projected onto an electrostatic potential isosurface.

The bond lengths, the angles between bonds, and the torsion angles of carbidopa molecule are the structural properties calculated in this work. Table 1 presents the comparative optimized structural parameters to the bond length of the carbidopa geometry. The theoretical values were analyzed by comparing the bond length generated by the LDA/PWC approximation with the GGA/PBE and GGA/BLYP approxi-

mations. Statistical analysis shows that the bond length calculated by GGA/PBE tends to increase by 0.55 %, while GGA/BLYP tends to decrease the length by 0.04%. As one can see in Table 1, the most pronounced increase in bond length occurs for the N5-N6 bond (about 2.4 % for the GGA/PBE), while the largest bond length decrease is observed for the N6-H21bond length (about 1.4 % for the GGA/PBE). On the other hand, the bond lengths granted by the GGA/BLYP are approximately 60 % the value found for the LDA-carbidopa case.

Table 1. Bond lengths (in Å) of the carbidopa molecule calculated through the LDA/PWC, GGA/PBE, and GGA/BLYP approximation methods.

Geometrical	Methods		
Parameters	LDA/PWC	GGA/PBE	GGA/BLYP
O1-C11	1.326	1.323	1.345
O1-H17	1.038	1.037	1.018
O2-C11	1.217	1.213	1.219
O3-C14	1.352	1.349	1.371
O3-H18	0.982	0.981	0.976
O4-C16	1.367	1.364	1.383
O4-H19	0.975	0.974	0.971
N5-N6	1.440	1.440	1.473
N5-H20	1.030	1.030	1.025
N6-H21	1.025	1.025	1.024
N6-H22	1.028	1.028	1.025
C7-N5	1.463	1.463	1.486
C7-C8	1.525	1.525	1.551
C7-C10	1.514	1.514	1.537
C7-C11	1.538	1.541	1.564
C8-C9	1.493	1.494	1.514
C8-H23	1.103	1.103	1.099
C8-H24	1.101	1.101	1.098
C9-C12	1.397	1.396	1.406
C9-C13	1.392	1.392	1.403
C10-H25	1.102	1.102	1.100
C10-H26	1.103	1.102	1.099
C10-H27	1.101	1.101	1.097
C12-C14	1.383	1.383	1.395
C12-H28	1.095	1.095	1.091
C13-C15	1.389	1.388	1.399
C13-H29	1.094	1.094	1.089
C14-C16	1.394	1.395	1.405
C15-C16	1.379	1.379	1.392
C15-H30	1.096	1.096	1.093

Table 2 is the second statistical analysis of the carbidopa, showing the angles between bonds of the molecule. It reveals that, in comparison with the LDA/PWC, the geometry optimized by GGA/PBE (GGA/BLYP) does not (does) change significantly, being the bond-bond angle in average greater (smaller) by 0.03 (0.14) degree of deviation. The largest variation to GGA/PBE and GGA/BLYP is 0.26 degree (for the H17-O1-C11 bond angle) and 1.94 (for the C7-C8-C9 bond angle) degrees, in that respective order. The most pronounced bond-bond angle decrease occurs for the O3-C14-C12 chain (at about 0.002 degree, GGA/PBE calculation) and the C10-C7-N5 chain (at about 0.075 degree, GGA/BLYP approximation).

Table 2. Angles between bonds (in degrees) of the carbidopa molecule calculated through LDA/PWC, GGA/PBE, and GGA/BLYP approximation methods.

Geometrical	Methods		
Parameters	LDA/PWC	GGA/PBE	GGA/BLYP
H17-O1-C11	106.972	107.228	107.398
O2-C11-C7	121.883	121.827	122.190
N5-C7-C11	116.144	116.043	116.528
N6-N5-C7	112.597	112.511	112.200
H20-N5-C7	107.813	107.879	107.013
H21-N6-H22	106.188	106.147	105.227
C10-C7-N5	108.816	108.793	108.741
C10-C7-C11	106.659	106.793	106.739
C10-C7-C8	110.047	110.027	109.310
C7-C8-C9	113.535	113.544	115.472
H23-C8-H24	108.784	108.716	107.998
H18-O3-C14	106.406	106.656	107.129
O3-C14-C12	121.263	121.261	119.808
H19-O4-C16	109.839	110.089	109.057
O4-C16-C15	125.241	125.356	124.725
C9-C13-C15	120.391	120.387	120.557
C12-C14-C16	119.452	119.410	119.530
C8-C9-C12	120.050	120.020	119.864

Finally, Table 3 shows the torsion angles involving groups of four atoms which are connected to three adjacent bonds. The carbidopa (calculated by the GGA/PBE functional) displays a smaller average increasing of the torsion angle, of about 0.76 degrees (difference of 4.29 %). On the other hand, the GGA/BLYP-carbidopa reveals a smaller average decreasing of the torsion (0.03 degrees). The latter result, in comparison with the LDA/PWC-carbidopa, shows that the changes in the molecule is smaller, being approximately 0.2 %, meaning that the GGA/BLYP is less distorted than the GGA/PBE case. There are four groups of atoms that are almost invariant to both GGA/LDA approximation, all of them belonging to the benzene ring, the reason for that being due to the fact that the benzene ring is very rigid [Pandey *et al*, 2001]. Therefore, the set of atoms with larger torsion angle variations are C7-C8-C9-C12 (3.4 degrees), C8-C9-C13-C15 (2.1 degrees), and C8-C9-C12-C14 (-2.3 degrees).

3.2 Charge Population Analysis

Table 4 presents the calculated electric charges for selected regions of the carbidopa molecule using Mulliken population analysis (MPA) [Mulliken, 1955], Hirshfeld population analysis (HPA) [Hirshfeld, 1977], and an electrostatic fitting of electric charges (ESP) [Singh *et al*, 1984]. The MPA analysis is limited, due to the arbitrary division of the overlap electron population. If the charge transfer is very small, Fukui function indices, estimated through the MPA analysis, are unpredictable sometimes [Roy *et al*, 2001]. Differently, the HPA

Table 3. Torsion angles (in degrees) of the carbidopa molecule calculated through LDA/PWC, GGA/PBE, and GGA/BLYP approximation. methods

Geometrical Parameters	Methods		
	LDA/PWC	GGA/PBE	GGA/BLYP
C8-C7-N5-N6	170.586	172.224	170.788
N5-C7-C8-C9	-54.945	-53.437	-55.095
N5-C7-C11-O1	-33.000	-32.042	-33.081
C7-C8-C9-C12	93.755	97.175	93.472
C8-C9-C12-C14	-177.894	179.787	-177.972
C8-C9-C13-C15	178.011	-179.857	178.102
C9-C12-C14-O3	-179.850	-179.800	-179.880
C9-C13-C15-C16	-0.356	0.194	-0.349
O3-C14-C16-O4	0.069	-0.029	0.099
C13-C15-C16-O4	179.966	179.690	179.945

analysis tends to be more accurate, producing more realistic Fukui function indices [Roy *et al*, 1999], [Parr *et al*, 1984], with good prediction of reactivity trends within a molecule in comparison to the MPA one [Mulliken, 1955], natural bond orbital (NBO) analysis [Foster *et al*, 1980], and methods that use the molecular electrostatic potential [Bonaccorsi *et al*, 1970]. Lastly, the HPA analysis tries to minimize the loss of information due to the joining of atoms to form a molecule [Ayers *et al*, 2002], [Nalewajski *et al*, 2000]. For this reason, we will focus our discussion mainly on the charges obtained from the HPA approach, followed by the MPA and ESP ones.

Table 4. Hirshfeld, Mulliken, and Electrostatic Fitting population analysis of the electric charges for the carbidopa molecule calculated through three DFT approximation methods.

Charges	LDA/PWC	GGA/PBE	GGA/BLYP
HPA NHNH2	+0.139	+0.112	+0.097
MPA NHNH2	-0.006	-0.025	-0.061
ESP NHNH2	-0.156	-0.172	-0.177
HPA COOH	-0.213	-0.201	-0.192
MPA COOH	-0.034	-0.026	-0.034
ESP COOH	-0.083	-0.079	-0.074
HPA PP	+0.073	+0.088	+0.096
MPA PP	-0.032	+0.002	+0.045
ESP PP	-0.032	+0.002	+0.045
HPA HD1	-0.030	-0.029	-0.039
MPA HD1	-0.144	-0.170	-0.197
ESP HD1	-0.091	-0.092	-0.109
HPA HD2	+0.016	-0.001	-0.014
MPA HD2	-0.199	-0.216	-0.242
ESP HD2	-0.113	-0.114	-0.130
HPA PH	+0.016	+0.032	+0.054
MPA PH	+0.416	+0.436	+0.492
ESP PH	+0.326	+0.315	+0.332

In order to perform the charge analysis, let us divide the carbidopa molecule in six regions as follow: the $NHNH_2$ group; the COOH carboxyl group; the propionic region (PP), C7-C8-H_2; the first hydroxyl group (HD1), O3-H18, connected to the C14 carbon atom of the ring; the second hydroxyl group (HD2), O4-H19, connected to the C16 carbon; and the phenyl ring (PH). For the carbidopa molecule calculated by the LDA/PWC approximation, the $NHNH_2$ group has an HPA charge of +0.139 and the MPA and ESP are both negative, being their charges respectively equal to -0.006 and -0.156. The MPA charge is in the middle of the HPA and ESP values, being the difference equal to ± 0.15 to each one. On the other hand, the COOH group has an HPA charge of -0.213, while the MPA and ESP charges are at about 84 % (charge of -0.034) and 61 % (charge of -0.083) less negative than the HPA one. The propionic region has a small positive charge of about 0.073 (HPA group), but the MPA and ESP analysis predict approximately the same value of negative charge, -0.032. The HD1 group has a negative charge of -0.030 (HPA) and the MPA and ESP charges are -0.144 and -0.091, respectivelly, where the MPA is much more negative than the ESP and HPA analysis, being the largest absolute value of charge for that group. The second hydroxyl group, unlike the HD1, has a small positive HPA charge of +0.016, but the other charges are predicted as negative: -0.199 and -0.113 (MPA and ESP, in that respective order). Finally, the phenyl ring is predicted as positively charged for the three population method analysed, with HPA charge of 0.016, whereas MPA and ESP charges are 0.416 and 0.326, being the greatest absolute value of the whole molecule. Considering all data, we conclude that the ESP and MPA values have a better correlation in comparison with the HPA-MPA and HPA-ESP combination, within the DFT-LDA/PWC approximation.

When the carbidopa is calculated through the GGA/PBE functional, the $NHNH_2$ and COOH groups become less charged for the LDA/PWC. The HPA charges for $NHNH_2$ changes to 0.097, while the COOH charge increases up to -0.192. The HPA charges for PP, HD1, HD2, and PH regions change by a very small amount, with the largest one observed for PH group, (from 0.416 in the LDA/PWC case, up to 0.496). By contrast, the PP group (by MPA and ESP analysis) and HD2 (by HPA analysis) change in value and in sign to +0.045, +0.045, and -0.014, respectively. The largest charges appeared on the PH group, been predicted by the MPA method. Last, looking to the GGA/BLYP approximation, the $NHNH_2$ and COOH present the charges, +0.112 and -0.201, that were predicted by the HPA analysis; so these groups are generally less electrically charged than the LDA/PWC group. The other regions have the HPA charges very close to the LDA/PWC case, with the largest difference occurring for the PP group (both MPA and ESP), that predict a charge of +0.002. The most significant positive charge, in contrast with carbidopa LDA/PWC, occurs at the MPA PH group.

3.3 Molecular Orbital Studies

Calculated highest occupied molecular orbital (HOMO) and lowest unoccupied molecular orbital (LUMO) [Fukui *et al*, 1952] are depicted in Fig. 3, while the density of states plots

(DOS and PDOS) are showed in Fig. 4. Analyzing the frontier region, neighboring orbitals are often closely spaced [Ramalingam *et al*, 2011]. In face of that, consideration of only the HOMO and LUMO orbitals may not yield a realistic description of the frontier molecular orbitals. The total electronic density of states (DOS) based on a linear interpolation in parallelepipeds formed by the points of the Monkhorst-Pack set, followed by the histogram sampling of the resultant set of band energies, were calculated using the DMol^3 program [Ackland, 1998], while the partial electronic density of states PDOS calculations are based on the Mulliken population analysis, allowing the contribution from each energy band to a given atomic orbital to be calculated.

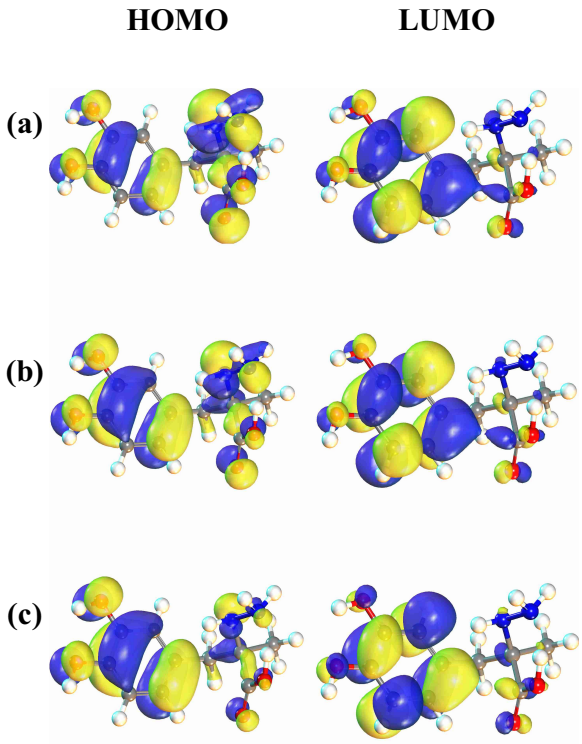

Figure 3. The highest occupied molecular orbital (HOMO) and the lowest unoccupied molecular orbital (LUMO) of the carbidopa molecule calculated by (a) DFT-LDA/PWC; (b) DFT-GGA/PBE; and (c) DFT-GGA/BLYP functionals of approximation.

Summation of these contributions over all bands produces a weighted DOS. The left-hand side plots of Fig. 4 (Figs. 4(a), 4(c), and 4(e)) are the PDOS diagrams, which show mainly the composition of the fragment orbitals contributing to the molecular orbitals, while on the right-hand side (Figs. 4(b), 4(d), and 4(f)) one can find the respective DOS diagrams. Both electronic density of states were calculated by three different quantum methods of simulation, namely the LDA/PWC, GGA/PBE, and GGA/BLYP functionals of the DFT theory. The PDOS represents useful semi-qualitative tools for analyzing the electronic structure. It further qualifies these results by resolving the contributions according to the angular momentum of the states. The most relevant contribution from C, N, and O atoms to the total electronic density of states on the Fermi energy is the 2p orbital for the three kinds of calculation, with maximum at -0.207 eV (LDA/PWC), -0.198 eV (GGA/PBE), and -0.196 eV (GGA/ BLYP). As one can see on the right-hand side of Fig. 4, the vertical dashed line represents the Fermi energy level, being -0.191 eV, -0.188 eV, and -0.184 eV the value predicted by the DFT-LDA/PWC, DFT-GGA/PBE, DFT-GGA/BLYP functionals, respectively.

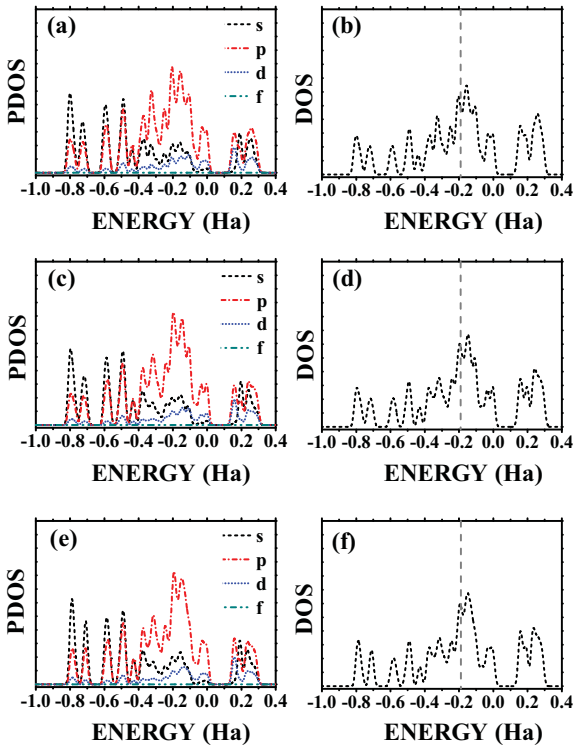

Figure 4. The predicted partial electronic density of states (PDOS, left-hand side) and the total electronic density of states (DOSl, right-hand side) of the carbidopa molecule calculated by DFT-LDA/PWC in (a) and (b); DFT-GGA/PBE in (c) and (d); and DFT-GGA/BLYP in (e) and (f) functionals of approximation. The vertical dashed line on the right charts indicate the Fermi energy measured in eV. The labels *s*, *p*, *d*, and *f* represent the atomic orbitals.

The energies for the HOMO, LUMO, and Δ(HOMO-LUMO) using LDA/PWC (GGA/PBE) calculation yield: -5.191, -1.164, and -4.027 (-4.978, -0.891, and -4.087) eV respectively. On the other hand, using the GGA/BLYP functional, the HOMO energy is -5.098 eV, the LUMO is -1.016 eV, and the Δ(HOMO-LUMO) is -4.082 eV, respectively. The energy gap of HOMO-LUMO explains the eventual charge transfer interaction within the molecule, which influences its biological activity. Consequently, the lowering of the HOMO-

LUMO band gap is essentially a consequence of the large stabilization of the LUMO due to the strong electron-acceptor ability of the elec-tron-acceptor group. The results show that the LDA/PWC variation of energy Δ(HOMO-LUMO) gives 4.027 eV in absolute value, which is about 0.060 and 0.055 eV smaller than the GGA/PBE and GGA/BLYP DFT functionals.

3.4 Optical Properties

We further calculate the optical absorption spectra of carbidopa using the LDA/PWC, GGA/PBE, and GGA/BLYP functionals of the DFT method. The single theoretical spectrum displayed in Fig. 5 refers to the DFT/GGA/PBE functional, from which one can see the labeled peaks of resonance. It depicts six peaks of absorption, where the biggest resonance one appears at 191 nm, while the smallest is observed at 296 nm. The remaining one are shown in the inset of Fig. 5 (we kept the DFT/GGS/PBE profile for comparison), being the LDA spectrum curve dashed red, the PBE spectrum curve solid black, and the BLYP spectrum curve point-dashed blue. Looking at the LDA curve, one can notice that the peaks are shifted backward, whose second peak of resonance is less intense and more prominent when compared to the PBE spectrum, which has the second peak located at 197 nm. By contrast, in the BLYP curve the peaks are shifted forward, and the second peak disappears when it is compared to the PBE curve. The major resonance peaks in all curves are assigned between 189-194 nm, and the energy of that peak is 6.48 eV.

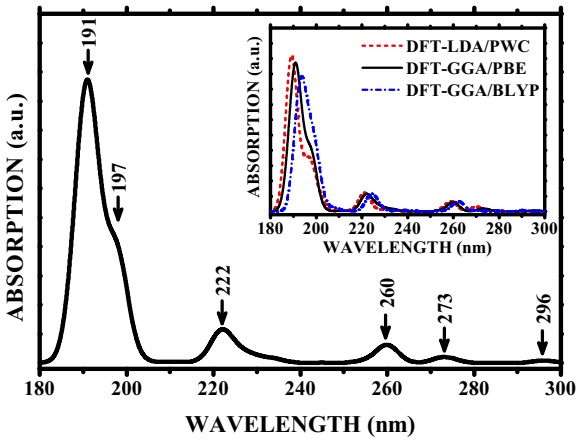

Figure 5. Optical absorption spectrum of carbidopa (with Gaussian broadening of 5.00 nm) calculated through GGA/PBE functional of DFT theory level. The peaks values of the resonance absorption peaks are labeled. The insert chart shows optical spectra calculated by LDA/PWC (dashed red line), GGA/PBE (solid black line), and GGA/BLYP (point-dashed blue line) functionals.

3.5 Vibrational Assignments

The carbidopa molecule consists of 30 atoms and does not belong to any specific group of symmetry. Hence, the number of normal modes of vibrations for carbidopa is 84. Out of the 84 fundamental vibrations, 76 modes are active both by IR absorption and Raman scattering, 7 modes are active only in IR, and just 1 mode is completely Raman. The harmonic-vibrational frequencies are calculated for carbidopa through DFT/B3LYP method using the triple split valence basis set, with the diffuse and polarization functions 6-311G(d,p).

In order to show the IR and Raman peaks, we have plotted in Figs. 6 and 7 the spectra profile for each kind of vibrational analysis. The IR intensity spectrum (Fig. 6) is divided into two parts, being Fig. 6(a) related to the wavevector for each peak from 0 until 2,000 cm^{-1}, while Fig. 6(b) shows the wavevector in the range 2,000-4,000 cm^{-1}. The Raman scattering spectrum was built up following the same procedure of the IR curve, with Fig. 7(a) depicting the wavevector from 0 to 2,000 cm^{-1} and Fig. 7(b) showing the peaks of activity between 2,000 and 4,000 cm^{-1}.

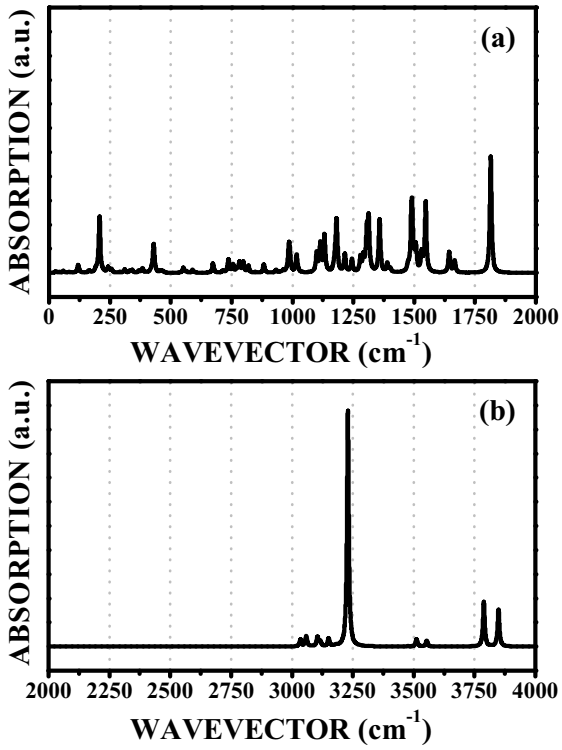

Figure 6. Theoretical calculated Infrared absorption spectrum of the carbidopa molecule at B3LYP/6-311G(d,p) basis set divided in two ranges of wavevector: (a) from 0 to 2,000 cm^{-1}, and (b) from 2,000 to 4,000 cm^{-1}.

3.5.1 C-H vibrations

Carbidopa molecule presents the carbon-hydrogen stretching vibration in the region 3,000-3,100 cm^{-1}, which is a characteristic region for the aromatic compounds [Holze, 1992], [Flakus *et al*, 2011]. Since carbidopa is a tri-substituted aromatic system, it has three bonds to complete the benzene ring. The expected three C-H vibrations corresponds to stretching

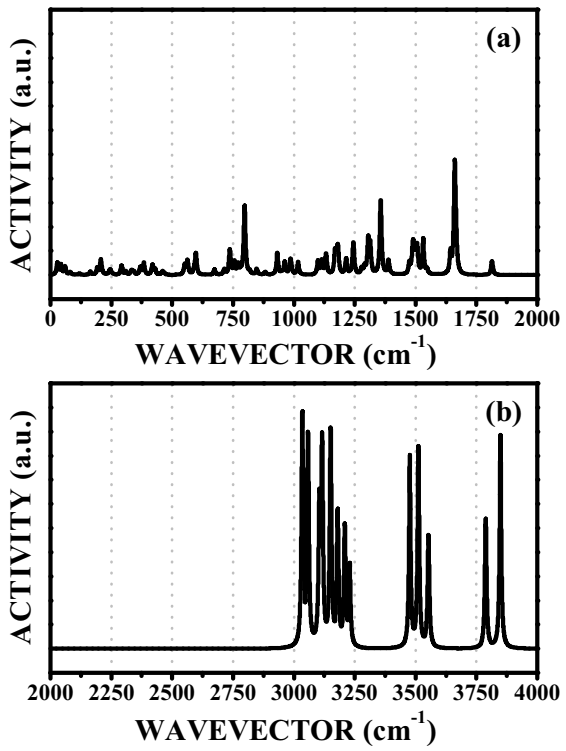

Figure 7. Same as in Figure 6 but for the calculated Raman scattering activity spectrum.

modes of C15-H30, C12-H28, and C13-H29 bonds. These vibrations are calculated at 3,150, 3,180, and 3,209 cm^{-1}, respectively.

The C-H out-of-plane bending mode usually appears in the range 670-950 cm^{-1}, and the C-H in-plane bending vibrations in the region 950-1,300 cm^{-1} [Yadav *et al*, 2006], [Silverstein *et al*, 1981]. In face of that, the C-H out-of-plane (C-H in-plane) bending vibrations are observed at 818, 882, and 950 (1,168, 1,181, and 1,214) cm^{-1}, respectivelly.

3.5.2 C=C vibrations

Basically the C=C stretching vibrations in aromatic compounds are observed in the region 1,430-1,650 cm^{-1} [Krishnakumar *et al*, 2009]. On the other hand, around the region 1,575-1,625 cm^{-1}, the presence of conjugate, such as C=C, causes a heavy doublet formation [Socrates, 2001]. The six ring carbon atoms go through coupled vibrations, known as skeletal vibrations, and in the region 1,420-1,660 cm^{-1} they give the maximum of four bands [Dani, 1995]. Because of that, the peaks at 1,305, 1,313, and 1,357 cm^{-1} are due to the strong C-C skeletal vibrations, while the peaks at 1,500, 1,547, 1,643, and 1,661 cm^{-1} are attributed to the strong C=C stretching on the carbidopa. The peaks at 1,305, 1,313, and 1,357 cm^{-1}, as well as the peaks at 1,500, 1,547, 1,643, and 1,661 cm^{-1} are due to the semicircle stretching and the quadrant stretching of C-C and C=C bonds, respectively. The peaks which are assigned at 468, 552, and 589 cm^{-1} are due to out-of-plane bending vibrations, and the peaks at 597, 674, and 755 cm^{-1} are due to C-C-C in-plane bending vibrations.

3.5.3 COOH vibrations

Carbonyl groups are sensitive, and both the carbon and oxygen atoms of the carbonyl move during the vibration with nearly equal amplitude [Siddiqui *et al*, 2010]. A single band was observed in the 1,814 cm^{-1} position, and this is due to the C=O stretching vibration. Nevertheless, the OH stretching band is characterized by a broadband appearing near 3,400 cm^{-1} [Sundaraganesan *et al*, 2007]. The band observed at the position 3,230 cm^{-1} is generated by the O-H stretching vibration.

The O-H out-of-plane and in-plane bending vibrations are usually observed in the regions 590-720 cm^{-1} and 1,200-1,350 cm^{-1} [Mahadevan *et al*, 2011]. In carbidopa, the O-H out-of-plane and in-plane bending vibrations are found at 988 cm^{-1} and 1,488 cm^{-1}, respectively. The peak in the Raman spectrum at 1,244 cm^{-1}, stronger than in the IR one, is assigned to the C-O stretching mode which is a pure mode. The C-O out-of-plane and in-plane bending vibrations for carbidopa are found at 419 cm^{-1} and 755 cm^{-1}, respectively.

3.5.4 Methyl group vibrations

The stretching vibrations on the C-H bonds of the methyl group are normally observed in the region 2,840-2,975 cm^{-1} [Socrates, 2001]. In the carbidopa molecule, there is strong bands around 3,034 cm^{-1} and around 3,104 cm^{-1}, corresponding to the symmetric and asymmetric stretching modes in the Raman spectrum, respectively. The C-H out-of-plane and in-plane bending vibrations for CH_3 methyl group in carbidopa are assigned at 755, 847, and 932 cm^{-1} and 1,401, 1,474, and 1,492 cm^{-1}, respectively. The C-CH_3 out-of-plane bending, in-plane bending, and stretching vibrations for carbidopa are found at 246, 310, and 1,114 cm^{-1}, respectively.

3.5.5 O-H vibrations

In a vibrational spectrum, the strength of hydrogen bond determines the position of O-H band [Siddiqui *et al*, 2010]. Normally the O-H stretching vibrations fall in the region 3,400-3,600 cm^{-1} [Krishnakumar *et al*, 2005]. Therefore, the theoretically computed stretching values for the O-H group is 3,230, 3,788, and 3,849 cm^{-1}, whereas the O-H out-of-plane and in-plane bending modes are observed at 1,643, 1,661, 1,814 cm^{-1} and 242, 459, 988 cm^{-1}, respectively, as pure mode of bending vibration. The two last peaks in the Raman spectrum are related with the stretching on the O-H group linked to the phenyl ring.

3.5.6 NHNH2 vibrations

The H-N stretching modes is more visible in the Raman activities spectrum, being localized around 3,500 cm^{-1}. The NH_2 symmetric and asymmetric stretching is observed at 3,476 and 3,553 cm^{-1}, respectivelly. The H atom of the H-N-N group, presents stretching vibration at 3,512 cm^{-1} and the N-N stretching is seen at 1,017 cm^{-1}. By contrast, the rocking mode is assigned in the range 28 and 43 cm^{-1}; the

wagging mode is found in the range 1,099-1,175 cm^{-1}; and the twisting vibration mode is observed from 1279 to 1356 cm^{-1}. The carbidopa compound presents two joined N nitrogen atoms. Therefore, there is a N-N stretching vibration mode on that molecule, being observed at 1,017 cm^{-1}, while the C-N stretching vibration appears at 1,175 cm^{-1}.

4. Conclusion

To summarize, we have performed a quantum chemical study of carbidopa using first-principle DFT approaches within the LDA/PWC, GGA/PBE, and GGA/BLYP exchange-correlation functionals. After carrying out a search for its optimal structure, we took into account the conformation of smallest energy (-793.66117 eV), from one of the nine geometries of smaller energies considered. The maximum bond distance difference between the calculated LDA/PWC structure and the GGA/PBE (GGA/BLYP) data is found for the N5-N6 (O2-C11), being +2.29% (PBE) and -0.33% (BLYP). On the other hand, the angles between bonds and torsion angles showed small variation when they were calculated by using the three quantum functionals considered in this work.

The population analysis was performed by three different methods (Hirshfeld, Mulliken, and Electrostatic Potential Fitting) to study the charge distribution of the carbidopa molecule. The positive and negative charge were located mainly at phenyl and hydroxyl groups, respectively. The largest positive (negative) charge observed was +492 (-242) predicted by MPA to the carbidopa molecule calculated through the GGA/BLYP functional. Comparing the charge sign, one can see that PBE and BLYP present the same behavior. Regarding PWC, only three signs on propionic (PP) and hydroxyl (HD) groups are different.

We calculated also the HOMO and LUMO molecular orbital to study the frontier orbitals. In average, the HOMO energy was about -5.089 eV, and the LUMO energy about -1.024 eV, giving Δ(HOMO-LUMO) equal to -4.065 eV, all of them predicted by the three different DFT functional approaches. To confirm these results, the total (DOS) and the partial (PDOS) electronic density of estates were analyzed. Besides, the Fermi energy level is -0.188 eV in average and the simulation predicted a density of states different of zero on the Fermi level. Meanwhile, observing the PDOS curves, one can realize that the most relevant contribution to the DOS was given by the 2p atomic orbital. The carbidopa conformer of smallest energy were also optimized using the B3LYP exchange- correlation functional and 6-311G(d,p) basis set to calculate their infrared intensity and Raman activity spectra, as well as to analyze its frequency assignments.

Finally, the exact identity of the carbidopa molecule was established, following a description which show, for instance, where absorption by single and double bonds are observed in the IR and Raman spectra. In the present work, the presence of the following groups was discussed: C=C, COOH, Methyl group, O-H and $NHNH_2$. Moreover, the different types of vibrations related to these groups (bending, in-plane and out-of-plane bending, stretching, symmetrical and asymmetrical stretching, twisting, scissoring and out-of-plane deformation by torsion) with their respective intensities, were identified and presented in Table 5. The calculated vibrational modes proved that the carbidopa molecule is stable (no imaginary frequency). Furthermore, one can identify that a very strong absorption peak, at 3,230 cm^{-1} (IR intensity), is related to the H17-O1 stretching vibration mode of the carboxyl group. On the other hand, the calculated Raman activity spectrum exhibits the most intense peak at 3,035 cm^{-1}, corresponding to the H-C symmetric stretching mode of the methyl group.

We strongly hope that, motivated by these and other progress, the theoretical predictions obtained here can be reproduced experimentally and that experimentalists get encouraged to face them.

Acknowledgments

This work was partially financed by the Brazilian Research Agencies CAPES (Rede NanoBioTec, PNPD), CNPq (INCT-Nano(Bio)Simes, Casadinho/Procad and PNPD) and FAPERN/CNPq-Pronex. The authors also thank CENAPAD/CE for providing the computational resources to perform the infrared and Raman spectra calculations using the Gaussian09 code.

References

[Lloyd *et al*, 1970] K.G. Lloyd and O. Hornykiewicz, *Parkinson's disease: activity of L-dopa decarboxylase in discrete brain regions*, Science **170**, 1213 (1970).

[Fahn *et al*, 1971] S. Fahn, L.R. Libsch, and R.W. Cutler, *Monoamines in the human neostriatum: topographic distribution in normals and in Parkinson's disease and their role in akinesia, rigidity, chorea, and tremor*, J. Neurol. Sci. **14**, 427 (1971).

[Frazao *et al*, 2012] N.F. Frazao, E. Albuquerque, U.L. Fulco, D.L. Azevedo, G.L.F. Mendonca, P. Lima-Neto, E.W.S. Caetano, J.V. Santana, and V.N. Freire, *Four-level levodopa adsorption on C60 fullerene for transdermal and oral administration: a computational study*, RSC Adv. **2**, 8306-8322 (2012).

[Calne, 1993] D.B. Calne, *Treatment of Parkinson's Disease*, New England Journal of Medicine **329**, 1021-1027 (1993).

[Gilbert *et al*, 2000] J.A. Gilbert, L.M. Frederick, and M. Ames, *The Aromatic-l-Amino Acid Decarboxylase Inhibitor Carbidopa Is Selectively Cytotoxic to Human Pulmonary Carcinoid and Small Cell Lung Carcinoma Cells*, Cli. Cancer Res. **6**, 4365-4372 (2000).

[Mazloum-Ardakani *et al*, 2011] M. Mazloum-Ardakani, B. Ganjipour, H. Beitollahi, M.K. Amini, F. Mirkhalaf, H. Naeimi, and M. Nejati-Barzoki, *Simultaneous determination of levodopa, carbidopa and tryptophan using nanostructured electrochemical sensor based on novel*

hydroquinone and carbon nanotubes: Application to the analysis of some real samples, Electrochim. Acta **56**, 9113-9120 (2011).

[Olanow *et al*, 2001] C.W. Olanow, R.L. Watts, and W.C. Koller, *An algorithm (decision tree) for the management of Parkinson's disease (2001):*, Neurology **56**, S1-S88 (2001).

[Nascimento *et al*, 2008] E.C.M. Nascimento, J.B. Martins, M.L. Santos, and R. Gargano, *Theoretical study of classical acetylcholinesterase inhibitors*, Chem. Phys. Lett. **458**, 285-289 (2008).

[Medeiros *et al*, 2007] S.K. Medeiros, E.L. Albuquerque, F.F. Maia Jr., E.W.S. Caetano, and V. Freire, *First-principles calculations of structural, electronic, and optical absorption properties of CaCO3 Vaterite*, Chemical Physics Letters **435**, 59-64 (2007).

[Kirkpatrick *et al*, 1983] S. Kirkpatrick, C.D. Gelatt, and M.P. Vecchi, *Optimization by Simulated Annealing*, Science **220**, 671-680 (1983).

[Stefan, 2004] G. Stefan, *Minima hopping: An efficient search method for the global minimum of the potential energy surface of complex molecular systems*, J. Chem. Phys. **120**, 9911-9917 (2004).

[Rappe *et al*, 1992] A.K. Rappe, C.J. Casewit, K.S. Colwell, W.A. Goddard, and W.M. Skiff, *UFF, a full periodic table force field for molecular mechanics and molecular dynamics simulations*, J. Am. Chem. Soc. **114**, 10024-10035 (1992).

[Casewit *et al*, 1992] C.J. Casewit, K.S. Colwell, and A.K. Rappe, *Application of a universal force field to organic molecules*, J. Am. Chem. Soc. **114**, 10035-10046 (1992).

[Casewit *et al*, 1992] C.J. Casewit, K.S. Colwell, and A.K. Rappe, *Application of a universal force field to main group compounds*, J. Am. Chem. Soc. **114**, 10046-10053 (1992).

[Rappe *et al*, 1993] A.K. Rappe, K.S. Colwell, and C.J. Casewit, *Application of a universal force field to metal complexes*, Inorg. Chem. **32**, 3438-3450 (1993).

[Delley, 1990] B. Delley, *An all-electron numerical method for solving the local density functional for polyatomic molecules*, J. Chem. Phys. **92**, 508-517 (1990).

[Delley, 2000] B. Delley, *From molecules to solids with the DMol3 approach*, J. Chem. Phys. **113**, 7756-7764 (2000).

[Hohenberg *et al*, 1964] P. Hohenberg and W. Kohn, *Inhomogeneous Electron Gas*, Phys. Rev. **136**, B864-B871 (1964).

[Kohn *et al*, 1965] W. Kohn and L.J. Sham, *Self-Consistent Equations Including Exchange and Correlation Effects*, Phys. Rev. **140**, A1133-A1138 (1965).

[Jones *et al*, 1989] R.O. Jones and O. Gunnarsson, *The density functional formalism, its applications and prospects*, Rev. Mod. Phys. **61**, 689-746 (1989).

[Gritsenko *et al*, 1997] O.V. Gritsenko, P.R.T. Schipper, and E.J. Baerends, *Exchange and correlation energy in density functional theory: Comparison of accurate density functional theory quantities with traditional Hartree-Fock based ones and generalized gradient approximations for the molecules Li[sub 2], N[sub 2], F[sub 2]*, J. Chem. Phys. **107**, 5007-5015 (1997).

[Dal Corso *et al*, 1996] A. Dal Corso, A. Pasquarello, A. Baldereschi, and R. Car, *Generalized-gradient approximations to density-functional theory: A comparative study for atoms and solids*, Phys. Rev. B **53**, 1180-1185 (1996).

[Fuchs *et al*, 1998] M. Fuchs, M. Bockstedte, E. Pehlke, and M. Scheffler, *Pseudopotential study of binding properties of solids within generalized gradient approximations: The role of core-valence exchange correlation*, Phys. Rev. B **57**, 2134-2145 (1998).

[Perdew *et al*, 1992] J.P. Perdew and Y. Wang, *Accurate and simple analytic representation of the electron-gas correlation energy*, Phys. Rev. B **45**, 13244-13249 (1992).

[Perdew *et al*, 1986] J.P. Perdew and W. Yue, *Accurate and simple density functional for the electronic exchange energy: Generalized gradient approximation*, Phys. Rev. B **33**, 8800-8802 (1986).

[Perdew *et al*, 1996] J.P. Perdew, K. Burke, and M. Ernzerhof, *Generalized gradient approximation made simple*, Phys. Rev. Lett. **77**, 3865-3868 (1996).

[Becke, 1988] A.D. Becke, *A multicenter numerical integration scheme for polyatomic molecules*, J. Chem. Phys. **88**, 2547-2553 (1988).

[Becke, 1993] A.D. Becke, *Density-functional thermochemistry. III. The role of exact exchange*, J. Chem. Phys. **98**, 5648-5652 (1993).

[Lee *et al*, 1988] C. Lee, W. Yang, and R.G. Parr, *Development of the Colle-Salvetti correlation-energy formula into a functional of the electron density*, Phys. Rev. B **37**, 785-789 (1988).

[Fast *et al*, 1999] P.L. Fast, J. Corchado, M.L. Sanchez, and D.G. Truhlar, *Optimized Parameters for Scaling Correlation Energy*, J. Phys, Chem. A **103**, 3139-3143 (1999).

[Frisch *et al*, 2009] M.J. Frisch, G.W. Trucks, H.B. Schlegel, and alet , Gaussian 09 Revision A.1; Gaussian Inc. Wallingford CT 2009.

[Santos *et al*, 2008] S.G. Santos, J.V. Santana, F.F. Maia Jr, V. Lemos, F.V. N., E.W.S. Caetano, B.S. Cavada, and E.L. Albuquerque, *Adsorption of Ascorbic Acid on the C60 Fullerene*, J. Phys. Chem. B **112**, 14267-14272 (2008).

[Zhao *et al*, 2005] Y. Zhao and D.G. Truhlar, *How well can new-generation density functional methods describe stacking interactions in biological systems?*, Phys. Chem. Chem. Phys. **7**, 2701-2705 (2005).

[Wijst van der *et al*, 2006] T. Wijst van der , C.F. Guerra, M. Swart, and F.M. Bickelhaupt, *Performance of various density functionals for the hydrogen bonds in DNA base pairs*, Chem. Phys. Lett. **426**, 415-421 (2006).

[Cooper *et al*, 2008] V.R. Cooper, T. Thonhauser, and D.C. Langreth, *An application of the van der Waals density functional: Hydrogen bonding and stacking interactions between nucleobases*, J. Chem. Phys. **128**, 204102 (2008).

[Silvestrelli, 2009] P.L. Silvestrelli, *van der Waals Interactions in Density Functional Theory Using Wannier Functions*, J. Phys, Chem. A **113**, 5224-5234 (2009).

[Ortmann *et al*, 2008] F. Ortmann, K. Hannewald, and F. Bechstedt, *Guanine Crystals: A First Principles Study*, J. Phys, Chem. B **112** (2008).

[Maia *et al*, 2011] F.F.J. Maia, V.N. Freire, E.W.S. Caetano, D.L. Azevedo, F.A.M. Sales, and E.L. Albuquerque, *Anhydrous crystals of DNA bases are wide gap semiconductors*, J. Chem. Phys. **134**, 175101 (2011).

[Ortmann *et al*, 2005] F. Ortmann, W.G. Schmidt, and F. Bechstedt, *Attracted by Long-Range Electron Correlation: Adenine on Graphite*, Phys. Rev. Lett. **95**, 186101 (2005).

[Ortmann *et al*, 2006] F. Ortmann, F. Bechstedt, and W.G. Schmidt, *Semiempirical van der Waals correction to the density functional description of solids and molecular structures*, Phys. Rev. B **73**, 205101 (2006).

[Kee *et al*, 2009] E.A. Kee, M.C. Livengood, E.E. Carter, M. McKenna, and M. Cafiero, *Aromatic Interactions in the Binding of Ligands to HMGCoA Reductase*, J. Phys, Chem. B **113**, 14810-14815 (2009).

[George *et al*, 1990] P. George and C.W. Bock, *A test of the AM1 model for calculating energies and structural properties of benzene, toluene, naphthalene, 1-methyl and 2-methylnaphthalene*, Tetrahedron **45**, 605-616 (1989).

[Pandey *et al*, 2001] R. Pandey, B.K. Rao, P. Jena, and M.A. Blanco, *Electronic Structure and Properties of Transition Metal-Benzene Complexes*, J. Am. Chem. Soc. **123**, 3799-3808 (2001).

[Mulliken, 1955] R.S. Mulliken, *Electronic Population Analysis on LCAO-MO Molecular Wave Functions. I*, J. Chem. Phys. **23**, 1833-1840 (1955).

[Hirshfeld, 1977] F.L. Hirshfeld, *Bonded-atom fragments for describing molecular charge densities*, Theor. Chem. Acc. **44**, 129-138 (1977).

[Singh *et al*, 1984] U.C. Singh and P.A. Kollman, *An approach to computing electrostatic charges for molecules*, J. Comput. Chem. **5**, 129-145 (1984).

[Roy *et al*, 2001] R.K. Roy, K. Hirao, S. Krishnamurty, and S. Pal, *Mulliken population analysis based evaluation of condensed Fukui function indices using fractional molecular charge*, J. Chem. Phys. **115**, 2901-2907 (2001).

[Roy *et al*, 1999] R.K. Roy, S. Pal, and K. Hirao, *On nonnegativity of Fukui function indices*, J. Chem. Phys. **110**, 8236-8245 (1999).

[Parr *et al*, 1984] R.G. Parr and W. Yang, *Density functional approach to the frontier-electron theory of chemical reactivity*, J. Am. Chem. Soc. **106**, 4049-4050 (1984).

[Foster *et al*, 1980] J.P. Foster and F. Weinhold, *Natural hybrid orbitals*, J. Am. Chem. Soc. **102**, 7211-7218 (1980).

[Bonaccorsi *et al*, 1970] R. Bonaccorsi, E. Scrocco, and J. Tomasi, *Molecular SCF Calculations for the Ground State of Some Three-Membered Ring Molecules: (CH[sub 2])[sub 3], (CH[sub 2])[sub 2]NH, (CH[sub 2])[sub 2]NH[sub 2][sup +], (CH[sub 2])[sub 2]O, (CH[sub 2])[sub 2]S, (CH)[sub 2]CH[sub 2], and N[sub 2]CH[sub 2]*, J. Chem. Phys. **52**, 5270-5284 (1970).

[Ayers *et al*, 2002] P.W. Ayers, R.C. Morrison, and R.K. Roy, *Variational principles for describing chemical reactions: Condensed reactivity indices*, J. Chem. Phys. **116**, 8731-8744 (2002).

[Nalewajski *et al*, 2000] R.F. Nalewajski and R.G. Parr, *Information theory, atoms in molecules, and molecular similarity*, Proc. Nat. Acad. Sci. **97**, 8879-8882 (2000).

[Fukui *et al*, 1952] K. Fukui, T. Yonezawa, and H. Shingu, *A Molecular Orbital Theory of Reactivity in Aromatic Hydrocarbons*, J. Chem. Phys. **20**, 722-725 (1952).

[Ramalingam *et al*, 2011] S. Ramalingam, P.D.S. Babu, S. Periandy, and E. Fereyduni, *Vibrational investigation, molecular orbital studies and molecular electrostatic potential map analysis on 3-chlorobenzoic acid using hybrid computational calculations*, Spectrochim. Acta, Part A **84**, 210-220 (2011).

[Ackland, 1998] G.J. Ackland, *Embrittlement and the Bistable Crystal Structure of Zirconium Hydride*, Phys. Rev. Lett. **80**, 2233-2236 (1998).

[Holze, 1992] R. Holze, *Spectroelectrochemical studies of the adsorption of 4-dimethylamino-4?-nitrostilbene on silver and gold electrodes*, Vib. Spectrosc. **3**, 255-263 (1992).

[Flakus *et al*, 2011] H. T. Flakus and B. Hachula, *Effect of the resonance of the C-H and O-H bond stretching vibrations on the IR spectra of the hydrogen bond in formic and acetic acid*, Spectrochim. Acta, Part A **79**, 1276-1284 (2011).

[Yadav *et al*, 2006] B.S. Yadav, S.K. Tyagi, and Seema, *Study of vibrational spectra of 4-methyl-3-nitrobenzaldehyde*, Indian J. Pure Appl. Phys. **44**, 644-648 (2006).

[Silverstein *et al*, 1981] R.M. Silverstein, Bassler, G. C., and T.C. Morrill John Wiley, New York, 1981.

[Krishnakumar *et al*, 2009] V. Krishnakumar, N. Surumbarkuzhali, and S. Muthunatesan, *Scaled quantum chemical studies on the vibrational spectra of 4-bromo benzonitrile*, Spectrochim. Acta, Part A **71**, 1810-1813 (2009).

[Socrates, 2001] G. Socrates John Wiley & Sons Ltd., Chichester, 2001.

[Dani, 1995] V. R. Dani Tata-McGraw Hill, 1995.

[Siddiqui *et al*, 2010] S.A. Siddiqui, A.K. Pandey, A. Dwivedi, S. Jain, and N. Misra, *Comparative conformational, structural and vibrational study on the molecular structure of tyrosine and L-DOPA using density functional theory*, J. Chem. Pharm. Res. **2**, 835-850 (2010).

[Sundaraganesan *et al*, 2007] N. Sundaraganesan, B. D. Joshua, and K. Settu, *Vibrational spectra and assignments of 5-amino-2-chlorobenzoic acid by ab initio Hartree-Fock and density functional methods*, Spectrochim. Acta, Part A **66**, 381-388 (2007).

[Mahadevan *et al*, 2011] D. Mahadevan, S. Periandy, and S. Ramalingam, *Vibrational spectroscopy (FTIR and FTRaman) investigation using ab initio (HF) and DFT (B3LYP) calculations on the structure of 3-Bromo phenol*, Spectrochim. Acta, Part A **78**, 575-581 (2011).

[Krishnakumar *et al*, 2005] V. Krishnakumar and R. Ramasamy, *Vibrational spectra and potential energy distributions for 4,5-dichloro-3-hydroxypyridazine by density functional theory and normal coordinate calculations*, Spectrochim. Acta, Part A **61**, 2526-2532 (2005).